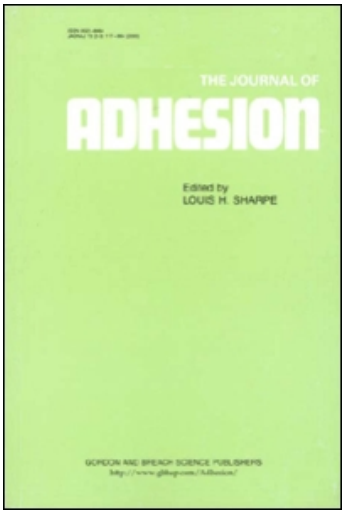

The Journal of Adhesion
Publication details, including instructions for authors and subscription information:
http://www.informaworld.com/smpp/title~content=t713453635

ADHESION FORCES OF SPHERICAL ALUMINA PARTICLES ON CERAMIC SUBSTRATES

Martin Götzinger[a]; Wolfgang Peukert[b]
[a] Institute of Particle Technology, Friedrich-Alexander-Universität, Erlangen, German [b] Institute of Particle TechnologyTechnische Universität München, Garching, German

Online publication date: 18 June 2010

To cite this Article Götzinger, Martin and Peukert, Wolfgang(2004) 'ADHESION FORCES OF SPHERICAL ALUMINA PARTICLES ON CERAMIC SUBSTRATES', The Journal of Adhesion, 80: 3, 223 — 242
To link to this Article: DOI: 10.1080/00218460490279297
URL: http://dx.doi.org/10.1080/00218460490279297

The Journal of Adhesion, 80: 223–242, 2004

ISSN: 0021-8464 print/1545-5823 online
DOI: 10.1080/00218460490279297

Taylor & Francis
Taylor & Francis Group

ADHESION FORCES OF SPHERICAL ALUMINA PARTICLES ON CERAMIC SUBSTRATES

Martin Götzinger
Institute of Particle Technology, Friedrich-Alexander-Universität, Erlangen, Germany

Wolfgang Peukert
Institute of Particle Technology, Technische Universität München, Garching, Germany

Adhesion forces of spherical alumina particles on ceramic substrates were studied. Results of direct force measurements using an atomic force microscope (AFM) were compared with theoretical results of a new rod model and with molecular dynamic computer simulation. Spherical alumina particles were produced by a flame process. The particles were glued to cantilevers, and interaction forces were measured by the AFM. A significant reduction of adhesion forces due to adsorbed layers was observed. The interaction volumes were determined by AFM scanning using a soft cantilever. The measured interaction forces were compared with calculated forces using the Hamaker concept including an adsorbed surface layer and the determined interaction volume (rod model). It turned out that calculated adhesion forces, neglecting deformation, are smaller than measured ones. This problem can be overcome if deformation according to Hertz is included in the rod model. Even for such a hard material as alumina, deformation occurs in the contact zone, which was also observed in a molecular dynamic computer simulation.

Keywords: Particle adhesion; Alumina; Roughness; Molecular dynamics

Received 12 May 2003; in final form 11 November 2003.

Presented in part at the 26th Annual Meeting of the Adhesion Society. Inc., held in Myrtle Beach, South Carolina, USA, 23–26 February, 2003.

This work was supported by the Deutsche Forschungsgemeinschaft (DFG) and Technische Universität München. The author thanks Dr. Julian Gale for providing GULP and Dr. W. Smith for providing DLPOLY.

Address correspondence to Wolfgang Peukert, Friederich-Alexander-Universität Erlangen-Nürnberg, Lehrstuhl für Feststoff und Grenzflächenverfahrenstechnik, Cauerstrasse 4, 91058 Erlangen, Germany. E-mail: w.peukert@lfg.uni-erlangen.de

INTRODUCTION

Particle adhesion is of importance in many industrial processes such as agglomeration, particle deposition, polishing, cleaning, and powder handling. With the stunning development of nano- and biotechnology, the relevance of particle interactions in both the liquid and the gas phase is critically important. Alumina is a technical material used in many different applications, *e.g.*, medical implants, dental restorative material, low-wear coatings, ceramics, and cutting or abrasive tools. The interaction of oxide particles with a flat substrate is a complex interplay between van der Waals forces, ionic multipole forces, elastic and plastic deformations, and bridging of adsorbed molecules such as water. In many powder handling unit operations, and also in applications such as the lubricant-free combustion engine, the understanding of the adhesion mechanisms is essential. Systematic studies of particle adhesion using defined geometries, *e.g.*, spheres, are lacking, especially for alumina. Cooper *et al*. [1] modeled the adhesion force of a rough alumina particle on SiO_2 and Cu, and Larson *et al*. [2] measured the force of a spherical silica particle on a flat alumina crystal. Muir *et al*. [3] presented an interaction force study of alumina fibers in water with coadsorbed polyelectrolyte. The focus of the latter study was on the interaction of alumina with the adsorbed molecules.

We start by focusing on van der Waals forces. By inversion of an appropriate adsorption model, we are able to determine disperse interactions from adsorption measurements in the Henry region. The Hamaker constant and the surface energy are important material parameters for modeling adhesion of particles. Furthermore, the interaction volume and the contact area are important parameters that have to be determined, for example, by AFM imaging. In a continuum approach using the Hamaker concept to describe long-range forces, the measured geometry of the particles was approximated using a rod model including adsorbed water layers. The amount of adsorbed water and the OH-group density on alumina was determined by Fourier transform infra red (FTIR) and thermogravimetric-mass spectrometric (TG-MS) analyses. This model is able to predict adhesion forces of particles well but it cannot describe the force as a function of separation at small distances ($<5\,\text{nm}$). For this reason, molecular dynamic calculations are performed to understand adhesion on a molecular level.

We present results from both experimental and theoretical research of surface-controlled mechanisms like adhesion and adsorption of alumina. In our approach, adsorption and adhesion are treated as related phenomena. Synergy is gained since adsorption and adhesion affect

each other in the contact zone of the adhesion partners. Both phenomena are governed by molecular interactions.

EXPERIMENTAL

Adhesion force measurements and the determination of surface geometry were carried out with a commercial AFM (Nanoscope IIIa, Digital Instruments, Santa Barbara, CA USA). Standard V-shaped silicon nitride cantilevers (Olympus, OTR8, 100/200 μm length, 800 nm thickness; Olympies, Tokyo, Japan) were used. The force constants were determined using the "added mass method" with an accuracy of ±5%. For adhesion force measurements in defined atmosphere, the commercial liquid cell for the Nanoscope IIIa was used. Instead of liquids, the cell was flushed with pure nitrogen (Messer Griesheim, 5.0; Megger Griesheim, Krefeld, Germany). The flow was stopped when force–distance curves were recorded.

As shown in Figure 1, the adhesion force was calculated from the distance of the zero-force point after jump-in, and the jump-out point was multiplied by the spring constant ($F_{adh} = P_m \times k$). For a proper statistical analysis, force–distance curves were analysed at least 20

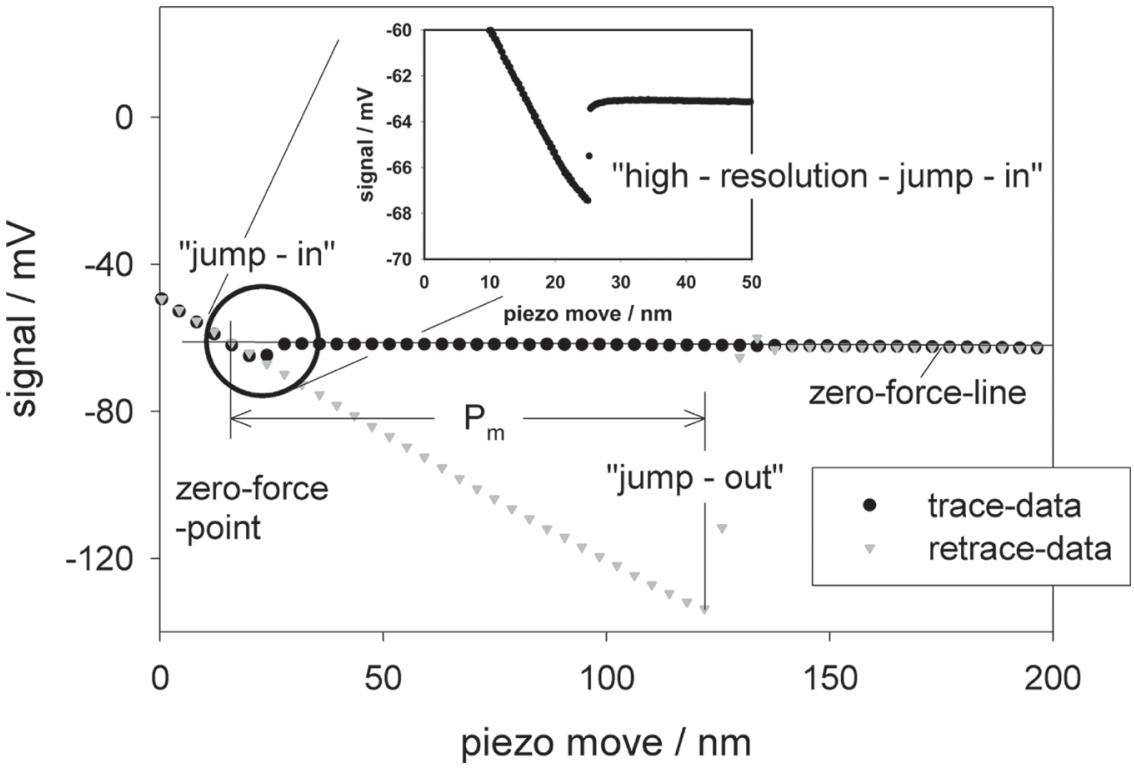

FIGURE 1 Measured force-distance-curve with low and high resolution. The adhesion force of a particle can be calculated by multiplying the distance, P_m, by the spring constant of the cantilever.

times at different positions. The standard deviation of adhesion forces with smooth substrates was much lower than with rough substrates.

For adhesion studies, smooth alumina and silica substrates (rms < 0.3 nm) and defined, rough silica substrates were used. To produce substrates with defined roughness, silicon wafers were coated by a dip-coating process. The substrates were immersed in three different coating sols containing monodisperse silica particles 30 nm, 110 nm, and 240 nm in size. The particle size was determined by a dynamic light-scattering technique in an ultra particle analyser (UPA, Microtrak; Honeywell, Phoenix, Arizona, USA). The substrates were withdrawn extremely slowly from the coating sol at a rate of 1 cm/day. At such slow velocity the deposition and drying stage are overlapping and regular, homogeneous mono- or bilayers of the nanoparticles can be produced in the case of 110 and 240 nm particles. However, when using the 30 nm sol a coating of approximately 200 nm thickness resulted. Figure 2 shows the AFM scans of the three substrates.

Details of the theory of structure formation were published by Günther and Peukert [4]. After the drying stage the coatings were sintered at 815°C for 15 min. This ensures that the nanoparticles keep a fixed position during the adhesion measurements. Due to the heat treatment, the surface chemistry of all silica substrates should be identical. The smooth substrates were also heated to 800°C to remove contaminations

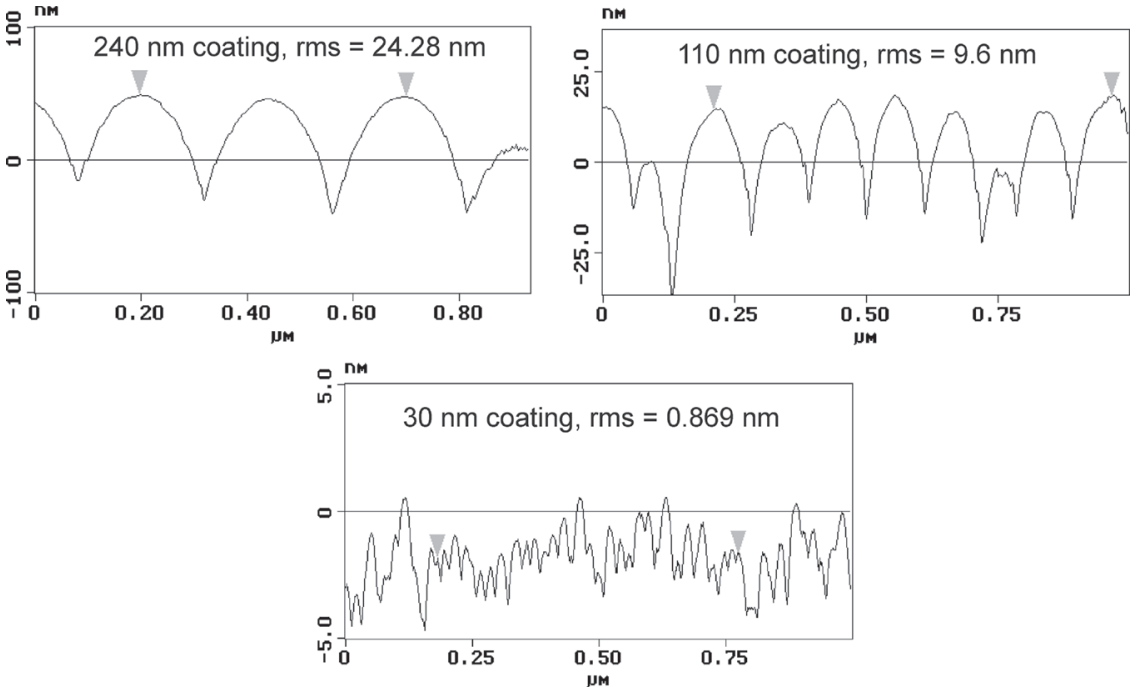

FIGURE 2 AFM scans of the substrates coated with 240, 110, and 30 nm silica particles. The rms values are 24.3, 9.6, and 0.87 nm, respectively.

and the OH groups. Immediately after heating, the samples were mounted on the AFM-piezo and flushed with pure nitrogen.

Smooth, spherical alumina particles with diameters between 2 and 30 μm were produced in a flame reactor. Details were described by Götzinger and Peukert [5]. After melting in the flame, the particles were collected on clean glass plates and then glued to AFM tips directly from these plates to avoid contamination and dust agglomeration. The particles are crystallized in the α-phase, which was determined by X-ray diffraction (XRD).

The interaction volumes of particles glued on stiff cantilevers were determined by AFM scanning using a soft cantilever. The particle-cantilever was positioned on the piezo showing the particle on the top and at an angle of 11° in order to scan the same sphere segment that was in contact with the substrates for the adhesion measurements. By this procedure, both the adhesion force and the interaction volume of the same particle can be determined. The interaction volume can be determined with nm resolution, much better than SEM imaging. Figure 3 shows a SEM picture and a cut of an AFM picture of the same alumina sphere. A kink can clearly be identified in both pictures.

Besides the particle geometry, the Hamaker constant and surface properties such as surface energy affect adhesion. Because it is not possible to determine the surface properties of a single particle glued to an AFM tip, different alumina (α- and δ-phase with and without OH groups) and dried silica sols (heated to 800°C) were analysed using TG-MS, FTIR, and adsorption. It is assumed that similar thermal pretreatment leads to similar surface properties. Similar to the inverse gas chromathography (iGC) method, adsorption measurements

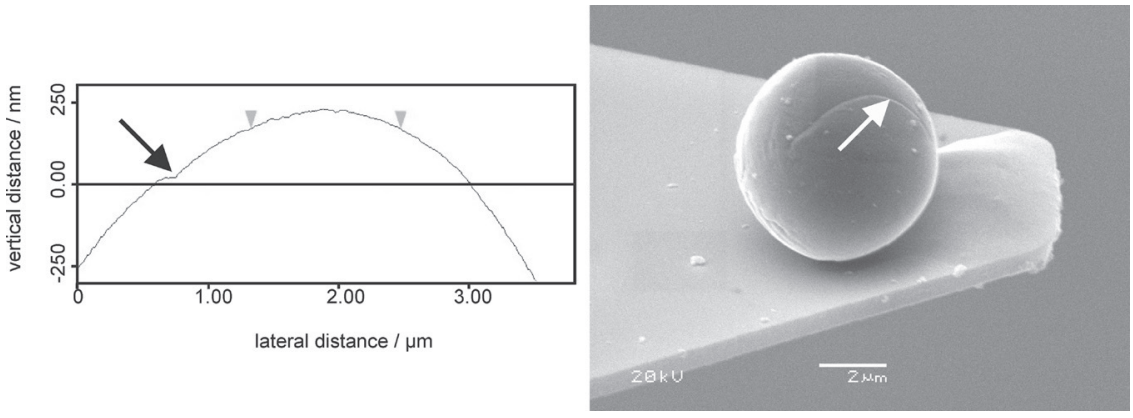

FIGURE 3 SEM image of an alumina particle (d = 6.0 μm) glued to an AFM cantilever (right). Cut of an AFM scan of the same particle (left). A kink on the particle surface is marked in both pictures.

in the Henry region can be used to determine surface interactions of particles. Powders with BET surface areas between 8.8 and 110 m^2/g were analysed. Single-component adsorption equilibria of gases such as Ar, Kr, Xe, CH_4, and C_4H_{10} were measured by a gravimetric method. An essential part of the adsorption setup is a Sartorius Ultramicro Balance (Sartorius GmbH, Type 7014, Göttingen, Germany, with an accuracy of $\pm 1\,\mu g$). The amount of adsorbed gas or vapour was determined from the variation of the sample weight due to rising pressure in a sealed volume after reaching equilibrium. To correct for buoyancy effects, the sample volume was determined by the Helium method. From these results the dispersion part of the surface energy can be determined. Interaction of water is also important because oxides are covered by a water layer at ambient conditions. For measuring the adsorption of water in the Henry region, a defined amount of water was injected into a gas bag to achieve a well known water partial pressure. OH group and water surface density were determined by TGA-MS and FTIR spectroscopy. Details of these measurements were published previously [6].

Molecular Dynamic Computer Simulations

We used the molecular dynamic software DLPOLY 2.12 whose Fortran 90 source code was developed by W. Smith and T. R. Forester at Daresbury Laboratory [7]. The Verlet-Leapfrog algorithm is used to solve the equations of motion of the atoms numerically. The simulations were performed using a timestep of 5 fs in the (N, p, T) or the (N, p, E) ensemble. The temperature was controlled by a Nosé-Hooverthermostat [27].

The interaction of an alumina particle with a flat alumina substrate was simulated. The potential used for alumina was originally developed by Lewis and Catlow [8]. Electronic polarisability of the oxygen ions was included *via* the shell model of Dick and Overhauser [9]. The potential of alumina was tested using the energy minimisation package GULP [10]. The potential parameters that describe interactions between water and alumina were taken from Leeuw and Parker [11].

RESULTS AND DISCUSSION

Influence of Adsorbed Layers

Alumina and silica are high surface energy materials. For instance, the mean surface energy of a clean alumina surface was experimentally determined to be 2.6 $J\,m^{-2}$ by means of calorimetry [12]. Theoretically,

Baudin and Hermansson [13] found a value of $3.2\,\mathrm{J\,m^{-2}}$ for the (0001 s) surface using molecular dynamic simulations. In ambient conditions, water and hydrocarbons adsorb on oxides because the systems tend to reduce the high surface energy. In the TG-MS analysis of our samples, the most important weight fraction of the removed components was water [6]. Hydrocarbons are also present, but their weight fraction can be neglected. In pure nitrogen a mean coverage of 1–2 monolayers of water (or OH groups) on alumina can be calculated from the weight loss and the BET surface area. This water can only be desorbed by heating to temperatures higher than 300°C.

The adsorbed layers reduce the surface energy of oxides by one up to two orders of magnitude. Adsorption is an appropriate method to determine the dispersive part of the surface energy, γ^d, or a Hamaker constant, A, of small particles. Hamaker constants of alumina were determined by inversion of an adsorption model derived by Maurer *et al.* [14]. As shown in Figure 4, the adsorption on δ-alumina in the Henry region of nonpolar molecules like Ar or C_4H_{10} can be described by a Hamaker constant of $A = 12.3 \times 10^{-20}$ J. Using the relation $A = 24\ \pi$

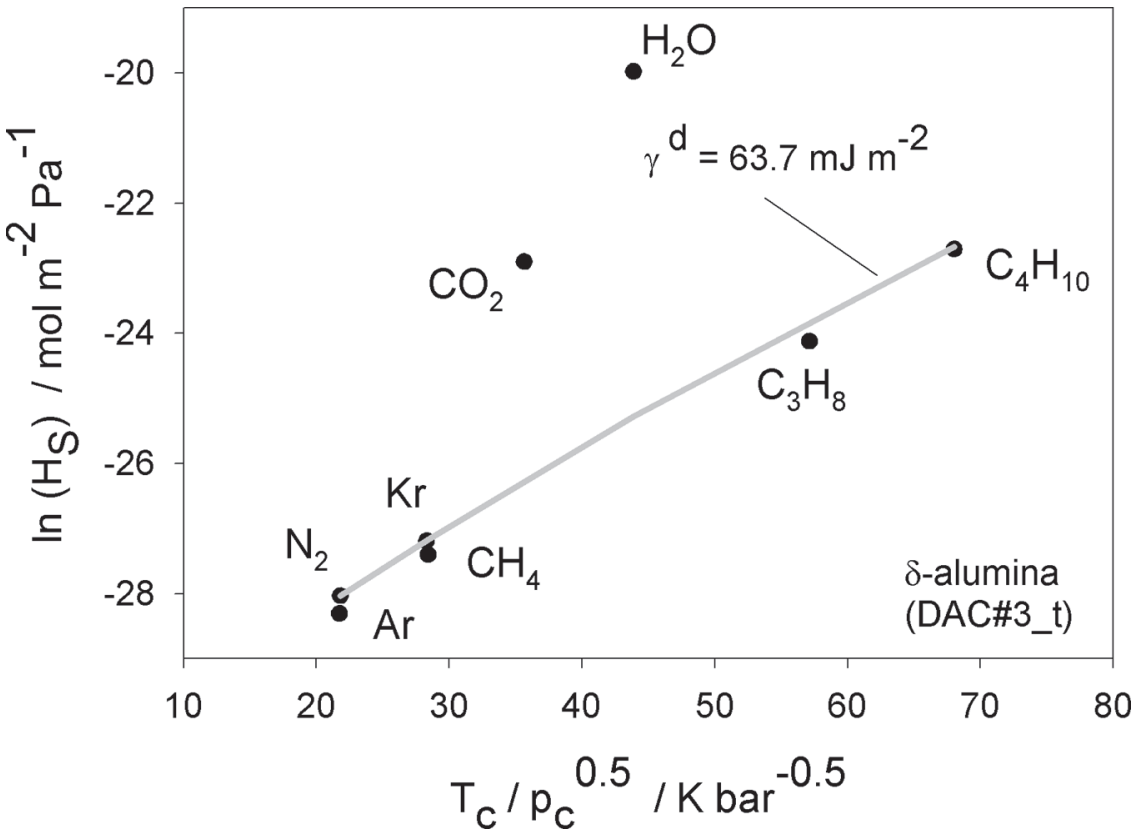

FIGURE 4 Measured Henry coefficients of different molecules on a δ-alumina. The adsorption of nonpolar molecules can be described using a dispersion surface energy of $\gamma^{\mathrm{d}} = 63.7\,\mathrm{mJ\,m^{-2}}$.

$a_0^2\ \gamma^d$ ($a_0 = 0.16\,\text{nm}$ according to Israelachvili [21]) and the Hamaker constant of $12.3 \times 10^{-20}\,\text{J}$, the dispersion surface energy of $\gamma^d = 63.7\,\text{mJ}\,\text{m}^{-2}$can be calculated for δ-alumina. For the dispersion surface energy of α-alumina we found $\gamma^d = 70.6\,\text{mJ m}^{-2}$ [16]. If polar interactions are important, *e.g.*, for CO_2 or H_2O, the Henry coefficients are larger. This larger interaction can be used to determine a mean charge due to an extended model, where quadrupole interactions are included [15]. The surface energy for water on alumina is larger than the dispersion part of $\gamma^d = 63.7\,\text{mJ m}^{-2}$, and it depends on the water coverage on the alumina surface. The surface energy of bulk water ($72\,\text{mJ}\,\text{m}^{-2}$) is a lower limit of the surface energy of water on alumina.

The adsorption method to determine Hamaker constants is affected by the thermal pretreatment of the samples. The measured Hamaker constant for α-alumina $A_{a,a} = 15.2 \times 10^{-20}\,\text{J}$ is in excellent agreement with the Lifshitz theory ($15 \times 10^{-20}\,\text{J}$) if the alumina surface is mostly water- and OH-group free, which can be achieved by heating [16]. If water or OH groups cover the surface, the effective Hamaker constant is smaller than the Lifshitz value.

The reduction of surface energy due to adsorbed layers affects particle adhesion. This result coincides with the observation in industrial powder-handling systems where the flowability of high surface energy powders may be improved by the addition of a small amount of water. The surface energy can also be reduced by adsorption of hydrocarbons, *e.g.*, butane. In Figure 5, adhesion measurements of a 6 μm particle on a smooth alumina substrate in pure nitrogen and in butane are compared. At a partial pressure of 1 bar for butane, approximately one monolayer of butane is adsorbed on alumina. This monolayer reduces the surface energy and, thus, the mean adhesion force from 542 nN to 434 nN, *i.e.*, by approximately 20%. The adsorbed layers are also responsible for the small difference of the adhesion forces between silica and alumina. Without thermal pretreatment, similar adhesion forces are measured on smooth silica and alumina substrates. Adhesion forces on thermally cleaned oxides (800°C) are closer to the expected forces for pure silica and alumina. For the interaction between silica ($A_{s,s} = 6.0 \times 10^{-20}\,\text{J}$) and alumina ($A_{a,a} = 15.0 \times 10^{-20}\,\text{J}$) a mean Hamaker constant of $A_{s,a} = 9.5 \times 10^{-20}\,\text{J}$ can be determined. Using this value and $A_{a,a} = 15.0 \times 10^{-20}\,\text{J}$ for alumina, a factor of 1.6 difference for the adhesion force on the alumina substrate compared with the value on the silica substrate is expected, which is larger than the measured factor of 1.3. The effect of contamination due to adsorbed layers must not be neglected, and samples have to be pretreated in the same way to obtain comparable adhesion measurements for different particles.

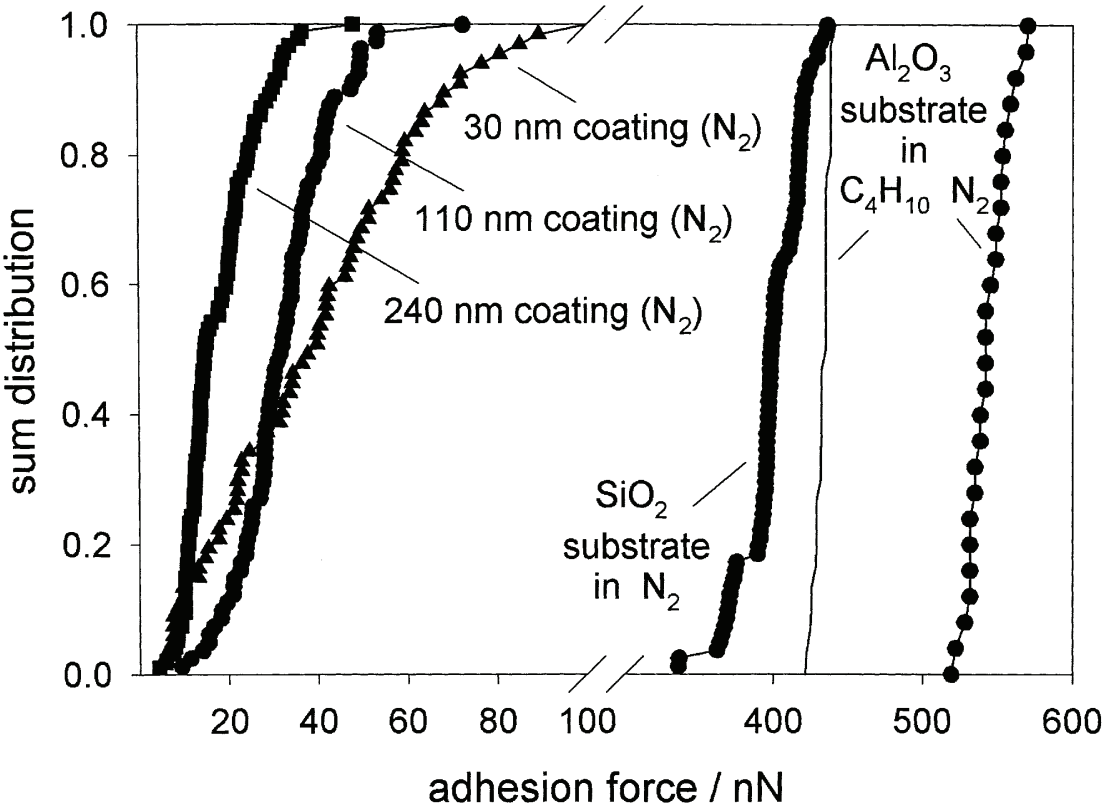

FIGURE 5 Sum distribution function of the adhesion forces of a 6.0 μm alumina particle interacting with a smooth alumina (in N_2 and C_4H_{10}) and a smooth silica substrate compared with silica substrates with defined roughness measured with an AFM in N_2.

Influence of Surface Roughness

Roughness effects on adhesion were studied using a smooth silica substrate and silica-coated silicon wafers with defined roughness. The adhesion forces of a 6.0 μm smooth alumina particle interacting with a smooth alumina and silica substrate, respectively, and with three coated silicon wafers were compared. The rms values of the coatings consisting of 30, 110, and 240 nm silica particles are 0.87, 9.6, and 24.3 nm, respectively. Adhesion forces should be most sensitive in this roughness range, as predicted from roughness models according to Rabinovich *et al.* [17] or Rumpf [18]. For the particle used ($R = 3\,\mu m$) μm) and a mean Hamaker constant for silica and alumina of $A_{s,a} = 9.5 \times 10^{-20}$ J, a minimum adhesion force of 2.0 nN can be achieved with an asperity radius of 8 nm (or a coating made of 16 nm particles) according to the Rumpf model:

$$F_{\mathrm{Rumpf}}(a) = \frac{A}{6}\left[\frac{r}{a^2} + \frac{R}{(a+r)^2}\right]. \qquad (1)$$

The contact distance a was assumed to be a = 0.3 nm. For our 30, 110, and 240 nm coatings, the adhesion forces are predicted to be 2.8 nN, 9.7 nN, and 22 nN, respectively. The Rumpf model predicts minimal adhesion forces between a rough sphere and a flat surface since it assumes a minimal material density in the contact region.

Adhesion forces of the 6 μm particle were measured at 100 different positions on each substrate. By this procedure, an adhesion force distribution can be measured. As shown in Figure 5, the measured minimum values of the adhesion forces are 5.4 nN, 9.4 nN, and 5.9 nN for the 30, 110, and 240 nm coatings, respectively. The minimum adhesion forces are in the same order of magnitude as predicted from the Rumpf model, which considers only a single asperity and, thus, a single contact point. These small adhesion forces are observed only at some special positions; the mean values of the adhesion forces are not affected by roughness as strongly as predicted. On the coated substrates, many asperity particles are interacting with the larger alumina particle glued to the cantilever. Thus, not only a single but many contact points can form on rough substrates, depending on the lateral position and the deformation. The Rumpf model does not take into account these many points. The mean values on rough substrates are approximately one order of magnitude smaller than the values on the smooth substrates. However, the roughness model of Rumpf predicts a decrease of two orders of magnitude, which can only be observed for the minimum adhesion forces.

Further, the smallest mean adhesion force was observed on the 240 nm coating. This surprising result might be explained by the easier formation of many point contacts for coatings with smaller diameters. Depending on the lateral position, up to 4 contacts may form, resulting in an increase of the adhesion force by a factor of 4, neglecting deformations and assuming mathematical spheres. This is in good agreement with the measured distribution of the relatively large 240 nm particles (see Figure 5). Adhesion forces vary by a factor of approximately 20 for the 30 nm coating. This large range can only be explained by the formation of more than 4 contact points or due to deformation or some small roughness of the alumina particle. To resolve this further investigations are ongoing.

It is important to notice that smooth substrates should be used if basic particle adhesion studies are performed, *e.g.*, to study the effect of particle size on adhesion. Alumina particles with different radii were glued to cantilevers and the adhesion forces on a smooth alumina substrate were measured in pure nitrogen. Capillary forces were not observed. The experimental results are compared with adhesion models in Figure 6.

The adhesion forces of particles with a different radius can be described reasonably well by an adsorbed layer model [5], that is, neglecting deformation and roughness. At a more detailed view, particles with the same radius can adhere quite differently eventhough the particles seem to be very smooth. Similar variations for silica particles were found by Heim *et al.* [19]. Geometry fluctuations in the nm range affect the adhesion force strongly. In analytical models describing particle adhesion, the particles are assumed to be spheres in a strict mathematical sense. The surface of real, crystalline spheres, even those made as ideal as possible, always show some defects [20]. To describe the particle interaction of a real, usually rough particle, an appropriate model is necessary.

Rod Model

Because molecular van der Waals forces decrease rapidly with separation distance, the geometry and, thus, the density of matter in the interaction volume dominates the particle interaction. This is commonly

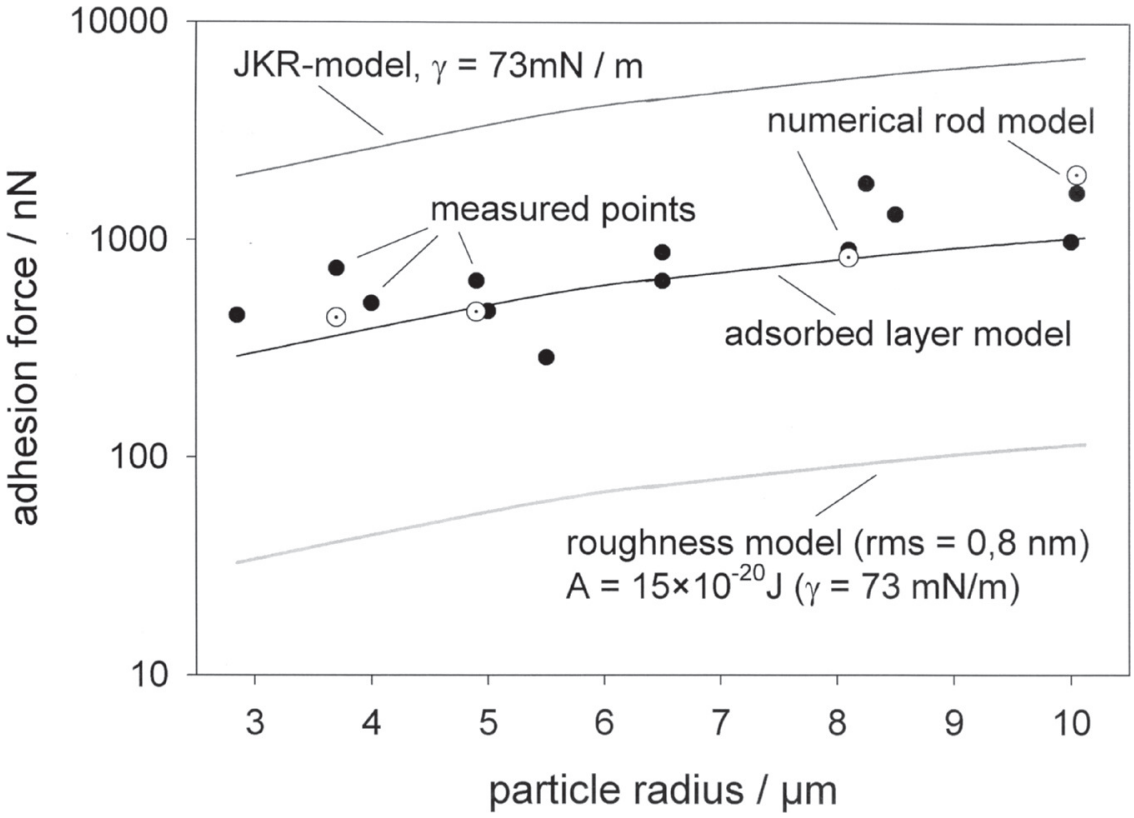

FIGURE 6 Adhesion forces of alumina spheres with different radii measured on a smooth alumina substrate in pure nitrogen.

expressed by the density theorem [21]. The relevant interaction volume for particle interaction comprises the interacting matter inside a 200–300 nm spacing between the interacting partners. The interaction volume and the roughness of the particles, whose adhesion force was already determined, were measured by AFM scanning, as described in the experimental section. As a result of the scan of the particle, a symmetric matrix, M, containing geometric information of the particle is obtained. The size of the matrix is defined by the scan resolution; we use 256×256 matrixes. Each matrix element, $M_{i,j}$ defines vertical position information, the lateral position of the matrix element, $M_{i,j}$ is defined by the scan size and the matrix indices i, j. As illustrated in Figure 7, the particle is approximated by rods above each matrix element of the scan. The lateral area of a rod is b^2, b depending on the scan resolution and the scan size. For a 3 μm scan and 256×256 points resolution, b is found to be $3\,\mu m/256 = 11.71\,nm$. It is assumed that the maximum of the scan and thus the maximum of

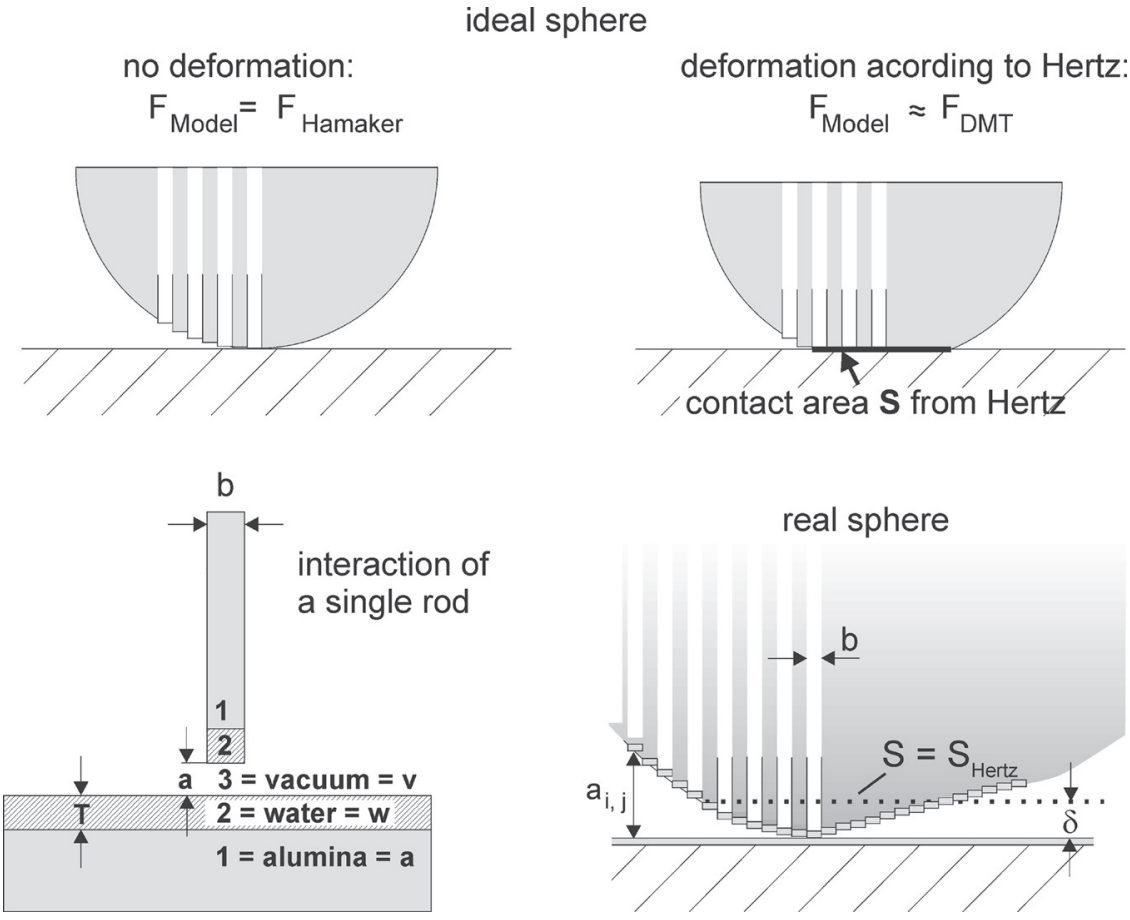

FIGURE 7 Rod model to calculate adhesion forces of particles. Validation by an ideal sphere (top) and application to real particles (bottom).

all matrix elements is in contact with the substrate. The distance between the individual rods, $a_{i,j}$, and the substrate is calculated by

$$a_{i,j} = \left(\mathrm{Max}(M_{i,j}) - M_{i,j}\right) + a_0, \tag{2}$$

with a_0 describing the minimal contact distance, set to 0.3 nm. It is assumed that the correct segment has been scanned and the point of the sphere that comes first into contact with the substrate is matrix-element Max $(_{i,j})$. Obviously, the matrix can be rotated easily and the interaction force of other geometric contacts can be calculated. Because the van der Waals forces fall rapidly with separation distance, it is a very good approximation to assume that the length of the rod reaches infinity. For a rod with infinite length interacting with a flat plate, an analytical expression is given by Israelachvili [21]. The force of the particle is the sum of the forces of all rods:

$$\begin{aligned} F_{i,j}^{\mathrm{rod}}(a_{i,j}) &= \frac{b^2}{6\pi}\left[\frac{A_{232}}{{a_{i,j}}^3} - \frac{A_{123}}{(a_{i,j}+T)^3} + \frac{A_{121}}{(a_{i,j}+2T)^3}\right]. \\ F_{\mathrm{particle}} &= \sum_{i,j} F_{i,j}^{\mathrm{rod}}. \end{aligned} \tag{3}$$

A layer with the thickness T is included, so that the interaction of oxides with adsorbed layers can be described. Using TG-MS, approximately one monolayer of water can be found on alumina; thus the thickness T was set to $T = 0.3$ nm, which is approximately the diameter of a water molecule. Using a Hamaker constant for water of $A_{w,w} = A_{22} = 3.7 \times 10^{-20}$ J and for alumina interacting across water of $A_{121} = A_{a,w,a} = 5.3 \times 10^{-20}$ J, and the mixing rule $A_{132} \approx \left(\sqrt{A_{11}} - \sqrt{A_{33}}\right) \cdot \left(\sqrt{A_{22}} - \sqrt{A_{33}}\right)$, the missing values in Equation (3) are estimated to $A_{w,v,w} = A_{232} = 3.7 \times 10^{-20}$ J and $A_{v,w,a} = A_{123} = -3.75 \times 10^{-20}$ J.

To validate the accuracy of the model, the adhesion force of an ideal, mathematical sphere was calculated from the model and the result was compared with the result from the Hamaker formula. Exactly the same result is obtained with the numerical method and the Hamaker formula. Using this rod model approach, the adhesion forces of real particles were calculated and compared with the measured values. It turned out that calculated forces were smaller than the measured forces. In the particle contact, the matter inside the interaction volume can be increased due to deformations. The increase of the contact area has an especially large impact on the adhesion force. This fact has to be considered. Unfortunately, the contact area, S, of hard oxide particles is difficult to determine experimentally and has been

calculated, *e.g.*, by the JKR approach [22] or the Hertz theory using the adhesive van der Waals pressure [23]. Both theories can be compared if the dispersion part of the surface energy, γ^d, is calculated from the Hamaker constant using the Frenkel relation $A = 24\pi a_0^2 \gamma^d$:

$$\begin{aligned} r_{cont}^{Hertz} &= \sqrt[3]{\frac{3F_{vdW}R}{4E^*}} = \sqrt[3]{\frac{3AR^2}{4\cdot 6E^* a_0^2}} = \sqrt[3]{\frac{3\cdot 24\pi\gamma^d a_0^2 \cdot R^2}{4\cdot 6E^* a_0^2}} \\ &= \sqrt[3]{\frac{3\pi\gamma^d R^2}{E^*}} \; r_{cont}^{JKR,sep} = \sqrt[3]{\frac{9\pi\gamma^d R^2}{4E^*}} \\ S = r_{cont}^2\pi \quad \delta = \frac{r_{cont}}{R} \quad & \frac{1}{E^*} = 2\cdot\frac{1-v^2}{E}, \end{aligned} \tag{4}$$

where E denotes the Young's modulus of alumina, F_{vdW} the van der Waals load, r_{cont} the contact radius, δ the deformation and R the particle radius. The contact radius of the JKR approach at separation is within a 15% deviation from the Hertz approach. We use the latter approach because our model is based on the use of Hamaker constants rather than surface energies. To calculate the contact area, S, it is assumed that the real particle can be approximated by an ideal sphere using $F_{vdw} = F_{adh}, F_{adh}$ being the measured adhesion force of the scanned particle. Including the deformation according to Hertz, the adhesion force of the particle is increased and can be calculated by:

$$\begin{aligned} &\bar{a}_{i,j} = a_{i,j} - \delta, \\ &F_{i,j} = \begin{cases} \dfrac{b^2}{6\pi}\left[\dfrac{A_{232}}{\bar{a}_{i,j}^3} - \dfrac{A_{123}}{(\bar{a}_{i,j}+T)^3} + \dfrac{A_{121}}{(\bar{a}_{i,j}+2T)^3}\right] & \text{for } \bar{a}_{i,j} \geq a_0 \\ \dfrac{b^2 A_{232}}{6\pi a_0^3} & \text{for } \bar{a}_{i,j} < a_0, \end{cases} \\ &F_{particle} = \sum_{i,j} F_{i,j}. \end{aligned} \tag{5}$$

For rods in contact, the contribution of A_{232} is dominant and A_{123} and A_{121} can be neglected. The area of all of the rods in contact is S.

This approach for calculating particle adhesion forces was validated using an ideal sphere. The result was within 10% accuracy of the value determined by the DMT model [24]. As shown in Figure 6, the measured adhesion forces are described well by our rod model.

To calculate the adhesion force of a rough particle with a flat plate, the lateral information of the position of each rod is unnecessary; only the value of the individual matrix elements, $M_{i,j}$, or rather the distance, $a_{i,j}$, determine the interaction force of a rod. Thus, it is sufficient

to consider only the frequencies of the values of $a_{i,j}$ and "forget" the lateral information of each matrix element. The elements, $a_{i,j}$, can be sorted and a frequency distribution function can be created. Other mathematical bodies can also be approximated by patches and a frequency distribution function of the separation distance, $a_{i,j}$, can be created. Doing so, the relevant geometric proportions of the scanned, real particle can easily be compared with idealized spheres, whose distribution functions are straight lines. In Figure 8, normalized to a projection area of $3 \times 3\,\mu m^2$, the distribution function of the scanned 5.9 μm particle (diameter) is compared with the distribution functions of mathematical spheres and a four-sided pyramid.

Next, the interaction of a 9.8 μm alumina sphere was measured in the noncontact region. As illustrated in Figure 1, only a few data points are available for the "jump-in" if a full force–distance curve is measured. By reducing the piezo movement range, data with an increased resolution can be measured, which we called "high resolution jump-in" measurement. It was expected that interaction forces at the jump-in can be described well by the rod model because no deformations occur here. In Figure 9 the experimental data are

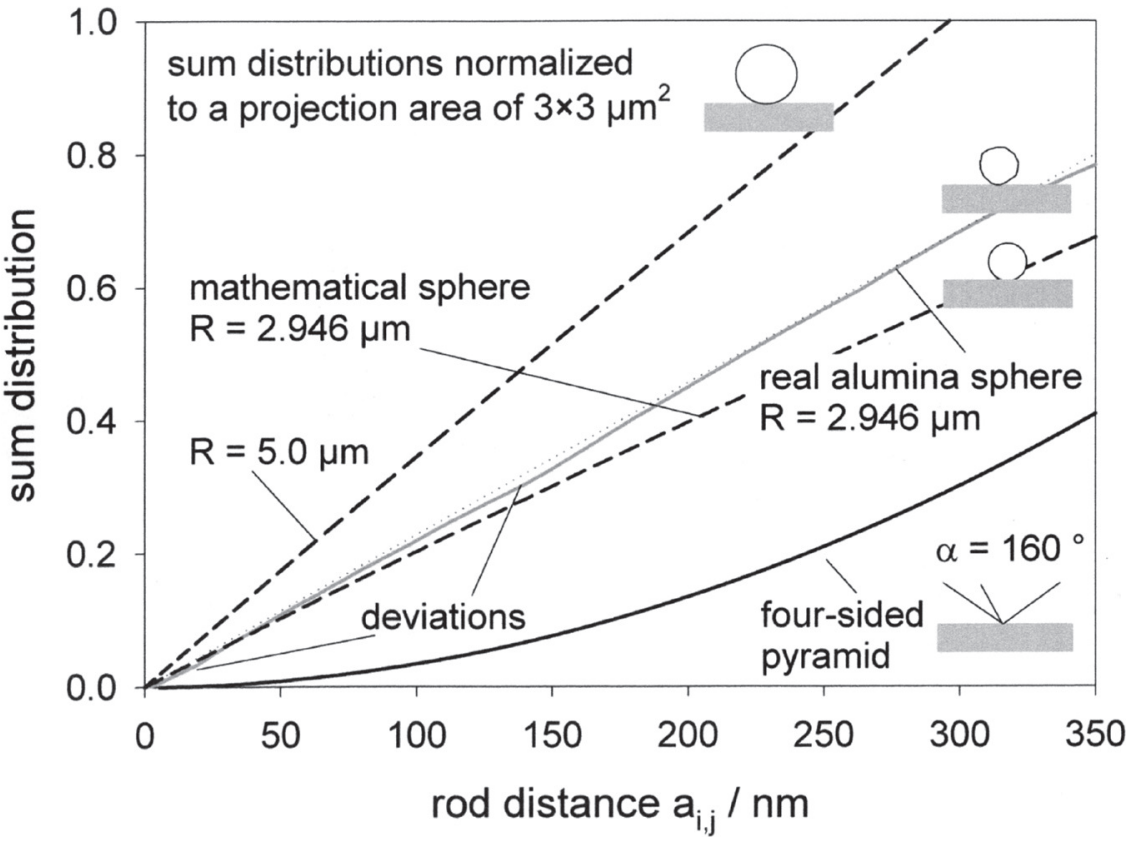

FIGURE 8 Frequency distribution of some model geometry compared with a real alumina sphere.

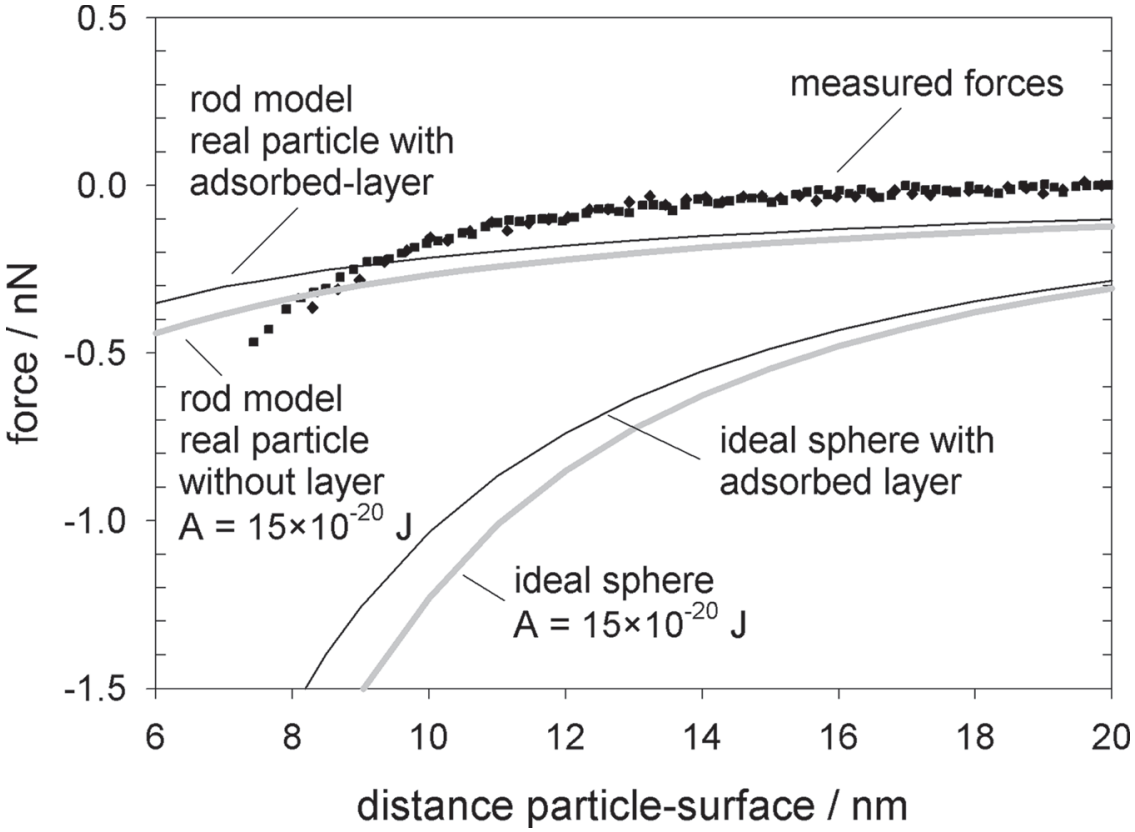

FIGURE 9 Interaction force of a 9.8 μm alumina sphere with a smooth alumina substrate compared with calculations.

compared with calculations using the rod model and the Hamaker formula, with and without an adsorbed water layer.

The distance of the particle from the surface was carefully calculated from piezo movement and cantilever deflection. One might argue that the substrate–sphere distance is not exactly known in AFM measurements due to deformations of the sphere or the glue between the sphere apex and the cantilever monitored with the laser, but the small force constant of the cantilever used here minimizes this effect. The measured forces are described reasonably well by the rod model at separations larger than 11 nm. However, the force progression at separations smaller than 11 nm cannot be explained by any continuum model. One possible reason is that the applied static view of the adhesion process might not be relevant.

Mobile surface molecules or atoms might accumulate in the gap, and the attractive interaction force can affect the atom positions near the apex. Both effects shorten the sphere–substrate distance. It is, therefore, highly desirable to use dynamic models to describe particle adhesion. One possibility is to use molecular dynamic (MD) simulations.

Molecular Dynamic Simulation

In our MD simulations, alumina is described by atomic force fields. The potential used was validated by energy minimisation. A density of 3.98 g /cm^3 (3.99 g /cm^3 in literature) and a Young's modulus of 403 GPa (370 GPa in literature) was calculated. Also, the mean static electronic polarisability was calculated to be 10.6, which is in very good agreement with the experimental value of 11.8. An alumina sphere (α-structure) with a radius of 0.9 nm was built. The cluster was simulated for 5 ps. As a result, an oxygen-terminated alumina cluster was formed while the α structure had changed to an amorphous structure. The alumina sphere was placed at a distance of 4 nm above the alumina plate (see Figure 10). A temperature of 300 K was chosen. The mass of the oxygen atoms of the upper part of the sphere and the bottom of the plate was increased to 1500 amu per atom to keep their position fixed. The forces were calculated, and results are shown in Figure 11. Each point is the result of a simulation for a system time of 0.2 ps, and a velocity of 2.5 Å /ps was applied. Due to the multipole forces of the oxygen-terminated alumina surface, the force is repulsive for large separation.

After contact, the interaction force is attractive due to rearrangement of the ions. The maximal force of 30 nN is two orders of magnitude

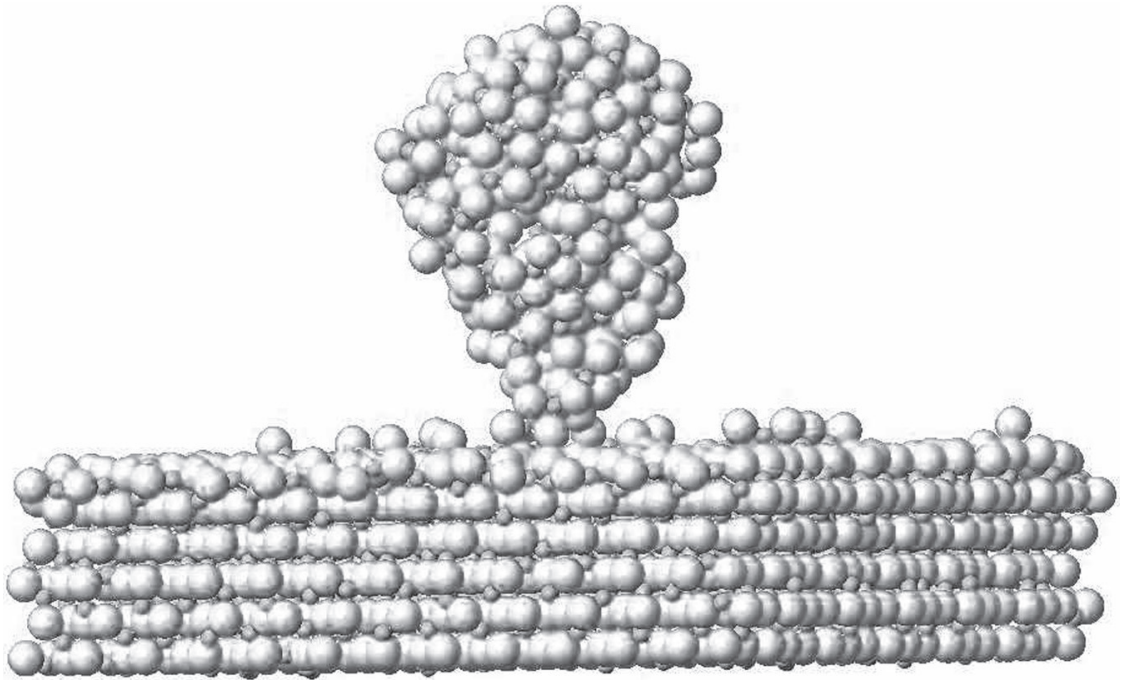

FIGURE 10 Alumina particle (r = 0.9 nm) in contact with an alumina plate in the pull off stage. The formation of a nano wire in the contact zone just begins.

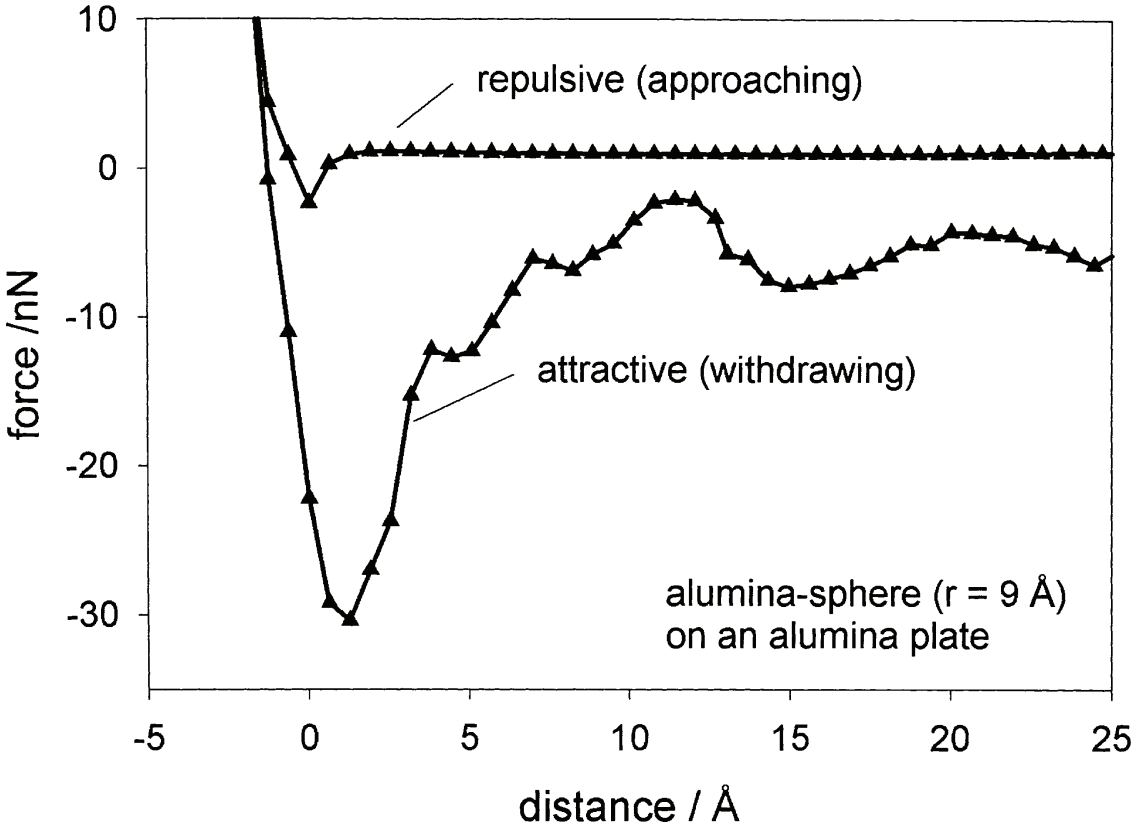

FIGURE 11 Calculated interaction force of a relaxed alumina particle (r = 0.9 nm) in contact with an alumina plate (result of the MD simulation).

larger than the van der Waals force. Using a surface energy of $3.2\,J\,m^{-2}$ for a water-free alumina surface and the DMT model [24] ($F = 4\pi\,R\,\gamma$) that is related to our rod model, an adhesion force of 36 nN can be calculated.

As shown in Figure 11, the force decrease shows steps due to the breaking of bonds. Large deformations occur and a long nanowire is formed. The formation of nanowires was also observed in MD studies of gold by Landman and Luedke [25]. In a recent simultaneous Transmission Electron Microscopy (TEM)-AFM study, the formation of a nanowire was proved experimentally in the contact of gold nanoparticles [26]. It seems that this nanowire formation is a general mechanism. However, no appropriate model is available yet that allows a description of this phenomenon (step-wise rip off). The understanding of the material rearrangement seems to be a key to understanding particle adhesion in the future.

Calculations that include a water layer on the alumina surface are ongoing. In a first simulation including a water layer, an adhesion force of 6 nN was calculated. As found experimentally, the adsorbed layer is dominating the particle adhesion force. The calculated

adhesion force is strongly affected by the water model used. For quantitative prediction of adhesion forces, the development of an appropriate water model is a key issue that will be included in the future.

CONCLUSION

The adhesion of oxide particles is complex since oxide surfaces are usually covered with adsorbed layers. Due to these layers, the total surface energy is reduced. Using MD simulations we were able to show that particle adhesion force is dramatically reduced if a water layer is adsorbed onto an alumina surface. The dispersion part of the surface energy of real particles can be determined from gas adsorption and is an order of magnitude smaller than the total surface energy. The surface energy of a real particle can be further reduced by adsorption of a low energy organic component like butane. Beside interaction force, geometry and roughness have a large impact on adhesion. The geometry of an irregularly shaped particle can be approximated by rods. The adhesion force can be calculated by a rod model where the total particle adhesion force is divided into surface forces and bulk forces. For using the correct surface force, deformation has to be considered even for such a hard material as alumina.

REFERENCES

[1] Cooper, K., Gupta, A., and Beaudoin, S., *J. Colloid Interface Sci.* **234**, 284–292 (2001).
[2] Larson, I., Drummond, C. J., Chan, D. Y. C., and Grieser, F., *Langmuir* **13**, 2109–2112 (1997).
[3] Muir, I., Meagher, L., and Gee, M., *Langmuir* **17**, 4932–4939 (2001).
[4] Günther, L. and Peukert, W., *Part. Part. Syst. Charact*. **19**, 312–320 (2002).
[5] Götzinger, M. and Peukert, W., *Powder Technol.* **130**, 102–109 (2003).
[6] Götzinger, M. and Peukert, W., Proceedings 26th Annual Meeting of the Adhesion Society, Myrtle, South Carolina, Beach, USA, 2003.
[7] Smith, W. and Forester, T. R., DLPOLY is a Package of Molecular Simulation Routines copyright: The Council for the Central Laboratory of the Research Councils, Daresbury Laboratory at Daresbury, Nr, Warrington, UK (2002).
[8] Lewis, G. V. and Catlow, C. R., *J. Phys. Chem.* **18**, 1149–1161 (1985).
[9] Dick, B. G. and Overhauser, A. W., *Phys Rev.* **120**, 90–103 (1958).
[10] Gale, J. D., *JCS Faraday Trans.* **93**, 629–637 (1997).
[11] Leeuw, N. H. and Parker, S. C., *J. Am. Ceram. Soc.* **82**, 3209–3216 (1999).
[12] McHale, J. M., Auroux, A., Perrotta, A. J., and Navrotsky, A., *Science* **277**, 788–791 (1997).
[13] Baudin, M. and Hermansson, K., *Surface Science* **474**, 107–113 (2001).
[14] Maurer, S., Mersmann, A., and Peukert, W., *Chem. Eng. Sci.,* **56**, 3443–3453 (2001).
[15] Götzinger, M., Mehler, C., and Peukert, W., *Annales Universitatis Mariae Curie-Sklodoeska* **LVII**, 140–157 (2002).

[16] Peukert, W., Mehler, C., and Götzinger, M., *Appl. Surface Sci.* **196**, 30–40 (2002).
[17] Rabinovich, Y. I., Adler, J. J., Ata, A., Singh, R. K., and Moudgil, B. M., *J. Colloid Interface Sci.* **232**, 10–16 (2000).
[18] Rumpf, H., *Chem.-Ing.-Tech.* **46**(1), 1–11 (1974).
[19] Heim, L. O., Blum, J., Preuss, M., and Butt, H. J., *Phys. Rev. Lett.* **83**, 3328–3331 (1999).
[20] Bausch, A. R., Bowick, M. J., Cacciuto, A., Dinsmore, A. D., Hsu, M. F., Nelson, D. R., Nikolaides, M. G., Travesset, A., and Weitztts, D. A., *Science* **299**,1716–1718 (2003).
[21] Israelachvili, J. N., 2nd ed., Academic Press, London, (1992), pp. 326–328.
[22] Johnson, K. J., Kendall, K., and Roberts, A. D., *Proc. R. Soc.* **A324**, 301–313 (1971).
[23] Rumpf, H., Sommer, K., and Steier, K., *Chem.-Ing.-Tech.* **48**(4), 300–307 (1976).
[24] Derjaguin, B. V., Müller, V. M., and Toporov, Y. R.,*Colloid Interface Sci.*, **53**, 314–326 (1975).
[25] Landman, U., Luedke, W. D., and Gao, J., *Langmuir*, 4514–4528 (1996).
[26] Erts, D., Löhmus, A., Löhmus, R., Olin, H., Pokropivny, A. V., and Ryen, L., and Svensson, K., *Appl. Surface Sci.* **188**, 460–466 (2002).
[27] Hoover, W. D., *Phys. Rev. A* **31**(3), 1695–1697 (1985).